journal

J. Am. Ceram. Soc., 88 [3] 742–749 (2005)
DOI: 10.1111/j.1551-2916.2005.00140.x

Finite Element Implementation of a Thermodynamic Description of Piezoelectric Microstructures

R. Edwin García†

Center for Theoretical and Computational Materials Science, National Institute of Standards and Technology, Gaithersburg, Maryland 20899-8500

Stephen A. Langer

Information Technology Laboratory, National Institute of Standards and Technology, Gaithersburg, Maryland 20899-8910

W. Craig Carter

Department of Materials Science and Engineering, Massachusetts Institute of Technology, Cambridge, Massachusetts 01239-4307

A model and numerical framework is developed for piezoelectric materials. The model treats the piezoelectric and electrostrictive effects by incorporating orientation-dependent, single-crystal properties. The method is implemented in Object Oriented Finite Element program, a public domain finite element code, so it can be applied to arbitrary two-dimensional microstructures with crystallographic anisotropy. The model is validated against analytic solutions. Consistency of the method for known cases permits application of the technique to more complicated two-dimensional systems. The piezoelectric and electrostrictive response is determined for a few simple device geometries and provides insight for design and convergence criteria.

I. Introduction

Progress towards optimal microstructures in high-performance electromechanical actuators and sensors depends, in part, on the development of novel materials, device architecture, amplification mechanisms, and processing techniques.[1] In piezoelectric materials, the effect of microstructure on the local state of stress and polarization is not simple to model because the fields are coupled, and the coupling is not necessarily spatially uniform. Furthermore, reliable models depend upon the proper incorporation of the physical properties at a microstructural level.

The spatial interactions of fields and material properties in a microstructure depend on fine-scale details. The macroscopic response may vary considerably for similar microstructures with the same microstructural parameters. To investigate the effects of microstructure on properties, two categorically different approaches may be considered: the fine scale effects can be spatially averaged and the microstructure approximated as a homogeneous material; or the spatial distribution of the properties of a particular microstructure can be incorporated into a complex model that treats all known interactions to the level of spatial resolution. The first, or homogenizing, approach will not describe those macroscopic properties that depend strongly on localized interactions but should be an economic method for calculation of those properties that depend on the mean of the microstructural distribution. In this paper, we describe a new method that adopts the second approach, which utilizes all available microstructural data.

Generally, the homogenization approach derives from fundamental work by Rayleigh,[2] Eshelby,[3] Hill,[4] Budiansky,[5] and Hashin.[6] For piezoelectric materials specifically, several homogenization approaches have been developed. Most of these methods are based on analytic solutions to electromechanical fields around a piezoelectric ellipsoidal inclusion.[7] The homogenization theory for composites containing piezoelectric inclusions is complex but has been successfully developed.[8–16] Another homogenization method, the multiple-scattering method, reduces the calculation of effective properties from a set of integral equations that derive from a Green's function to the superposition of a linear system of equations.[17]

However, if effects due to peculiarities of a *particular* microstructural feature (such as spatial correlations of crystallographic orientations, morphological texture, interface or boundary proximity effects, or defects such as pore and crack distributions) are to be calculated, homogenization approaches are very impractical. Homogenization methods that apply to cases where local variations in the microstructural fields are significant or have non-linear couplings (e.g., electrostriction, photoelasticity, electro-optic effects, etc.), would be useful, but are equally impractical. Moreover, when material response depends on improbable events or spatial correlations (e.g., when considering the reliability of piezoelectric devices with a dilute concentration of defects) homogenization approaches will not suffice.

The microstructural method reported in this paper provides a means to assess the effect of such correlations, non-linearities, and statistics. It can be used in samples with large spatial correlations or in materials that suffer the inadequacies of small number statistics, where the solution derived from the homogenization approach deviates greatly from the actual distribution of fields. The method is intended to improve processing design for devices, particularly when the device scale is similar to that of the microstructure or the relevant design feature depends on extremes of microstructural distributions.

Ultimately, piezoelectric function depends on the relationship between the spatial variations of the mechanical and electric fields as well as the anisotropy of the underlying single-crystal properties of each grain in a microstructure. It is not straightforward to develop criteria to determine which properties are confidently predicted by an effective medium approach and those that are directly related to localized interactions.

C. Randall—contributing editor

Manuscript No. 10592. Received October 14, 2003; approved May 10, 2004.
Supported by the MIT–Singapore Alliance and the Center for Theoretical and Computational Materials Science at the National Institute of Standards and Technology.
†Author to whom correspondence should be addressed. e-mail: redwing@alum.mit.edu

This paper describes a modeling framework for microstructural effects on complex piezoelectric microstructures. The framework is implemented with the finite element method and verified for simple geometries. The method is implemented in two dimensions (with plane stress and plane strain conditions). Numerical convergence with mesh size and direct applicability to simulations of device geometry are demonstrated. The analysis performed on the tested device geometries provides a set of simple guidelines for piezoelectric actuator design.

In a companion paper,[18] the numerical method is used to determine the effects of crystallographic texture in polycrystalline $BaTiO_3$ and PZN–PT.

II. Model Framework

(1) Equilibrium Equations and Constitutive Relations

If a non-piezoelectric phase undergoes a transition to a piezoelectric phase, the material's symmetry changes by the loss of an inversion center. In some cases, the piezoelectric phase transition induces a non-zero remnant strain and electric polarization. The magnitude of remnant strain can be reversibly changed with increased polarization and stress. If crystallographically equivalent remnant states of strain can be set by applying a very strong field, the material is called a ferroelectric.[‡]

It is possible to derive the conditions of local equilibrium of an electromechanical solid ($\nabla \cdot \overleftrightarrow{\sigma} = \vec{0}$; $\nabla \cdot \vec{D} = 0$) by minimizing a functional form of the total free energy.[21,22] The computational method presented in this paper follows directly from discretizing the variational formulation and substituting the electromechanical constitutive equations for each homogeneous region of a microstructure. The equilibrium equations are satisfied automatically when the discrete form of the free energy functional is minimized. With the free energy functional the computational method is reduced to specification of the constitutive equations, discretization, and subsequent numerical solution.

For the specification of electromechanical constitutive relations, mechanical and electrical fields are coupled through material properties:

$$\begin{aligned} \sigma_{ij} &= C^E_{ijkl}\varepsilon^{\mathrm{T}}_{kl} - C^E_{ijkl}d_{mkl}E_m \\ D_i &= \epsilon^{\overleftrightarrow{\varepsilon}^{\mathrm{T}}}_{ij}E_j + d_{ijk}C_{jklm}\varepsilon^{\mathrm{T}}_{lm} \end{aligned} \tag{1}$$

The symbols are defined in Table I. Each coefficient follows Nye's notation.[23]

For cases in which the material properties are also functions of applied fields, a higher order approximation is obtained by expanding the physical properties with respect to the intensive quantities:

$$\epsilon^{\overleftrightarrow{\sigma}}_{ij} = \epsilon^{\overleftrightarrow{\sigma},0}_{ij} + \gamma_{klij}\sigma_{kl} + \Lambda_{kij}E_k \tag{2}$$

$$d_{ijk} = d^0_{ijk} + \Gamma_{ijklm}\sigma_{lm} + \gamma_{ijkl}E_l \tag{3}$$

$$C^E_{ijkl} = C^{E,0}_{ijkl} + \chi_{ijklmn}\sigma_{mn} + \xi_{ijklm}E_m \tag{4}$$

In the limit of infinitesimally small changes with respect to equilibrium, the total strain can be expanded in terms of the contributions from each applied field:

$$\varepsilon^{\mathrm{T}}_{ij} \equiv \varepsilon^{\mathrm{elastic}}_{ij} + \varepsilon^{\mathrm{electric}}_{ij} + \cdots \tag{5}$$

[‡]Atomistically, the removal of an inversion center correlates with the directed displacement of one or several atoms in a unit cell. In most cases, the stress- and electric field-free directed displacement will occupy one of several equivalent crystallographic positions, called variants. If the directed displacement is induced by the application of an external field, then the system will switch to the variant that minimizes its free energy.[19,20]

Table I. Glossary of Symbols for Thermodynamic Properties

Summary of symbols for thermodynamic properties	
Definition	Name
C^E_{ijkl}	Stiffness tensor at constant electric field
$\vec{D}$	Total polarization or displacement vector
D_i	ith component of displacement vector
$\vec{E}$	Electric field vector
E_i	ith component of electric field
F	Total Helmholtz free energy
d_{ijk}	Piezoelectric tensor (d-form)
e_{ijk}	Piezoelectric tensor (e-form)
f	Helmholtz free energy density
u_i	ith component of the spatial displacement vector
Γ_{ijklm}	Electro-elastic tensor

Fifth rank tensor expressing linear correction to piezoelectric tensor due to change of stress. Zero for crystals with inversion center symmetry.

$$\Gamma_{ijklm} = \left.\frac{\partial d_{ijk}}{\partial \sigma_{lm}}\right|_{\overleftrightarrow{\sigma}_o, \vec{E}_o} \tag{29}$$

Λ_{kij}	Electro-optic tensor

Linear correction to dielectric response. This correction only exists in materials lacking an inversion center.

$$\Lambda_{kij} = \left.\frac{\partial \epsilon^{\overleftrightarrow{\sigma}}_{ij}}{\partial E_k}\right|_{\overleftrightarrow{\sigma}_o, \vec{E}_o} \tag{30}$$

Ω	Volume of solid
Ω_o	Reference volume
γ_{ijkl}	Photoelastic/electrostriction tensor

First-order correction to permittivity due to stress. Also electrostriction tensor, i.e., first-order correction to the piezoelectric tensor due to applied field $\vec{E}$.

$$\gamma_{ijkl} = \left.\frac{\partial \epsilon^{\overleftrightarrow{\sigma}}_{ij}}{\partial \sigma_{kl}}\right|_{\overleftrightarrow{\sigma}_o, \vec{E}_o} = \left.\frac{\partial d_{ijk}}{\partial E_l}\right|_{\overleftrightarrow{\sigma}_o, \vec{E}_o} \tag{31}$$

$\overleftrightarrow{\epsilon}^{\mathrm{T}}$	Dielectric permittivity tensor
$\epsilon^{\overleftrightarrow{\varepsilon}}_{ij}$	Dielectric permittivity at constant total strain

The dielectric permittivity at constant strain is related to the dielectric permittivity at constant stress through the relation [21]:

$$\epsilon^{\overleftrightarrow{\epsilon}^{\mathrm{T}}}_{ij} = (\epsilon^{\overleftrightarrow{\sigma}}_{ij} - d_{jmn}C^E_{mnkl}d_{ijkl}) \tag{32}$$

$\overleftrightarrow{\varepsilon}^{\mathrm{T}}$	Total strain tensor
$\varepsilon^{\mathrm{T}}_{ij}$	ijth component of total strain tensor
ξ_{ijklm}	Electric hardening tensor

Contribution to stiffness from induced polarization. Absent in centrosymmetric materials.

$$\xi_{ijklm} = \left.\frac{\partial C_{ijkl}}{\partial E_m}\right|_{\overleftrightarrow{\sigma}_o, \vec{E}_o} \tag{33}$$

$\overleftrightarrow{\sigma}$	Stress tensor
σ_{ij}	ijth component of stress tensor
ϕ	Electric potential
χ_{ijklmn}	Higher-order stiffness tensor

Reversible stress hardening coefficient.

$$\chi_{ijklmn} = \left.\frac{\partial C_{ijkl}}{\partial \sigma_{mn}}\right|_{\overleftrightarrow{\sigma}_o, \vec{E}_o} \tag{34}$$

The electric contribution to the total strain defines the piezoelectric coefficient tensor:

$$\varepsilon_{ij}^{\text{electric}} = d_{kij}E_k \tag{6}$$

Substituting Eq. (3) in Eq. (6) and defining $\varepsilon_{ij}^{\text{electrostrictive}}$ as the quadratic contribution to strain yields:

$$\varepsilon_{ij}^{\text{electrostrictive}} = \gamma_{ijkl}E_lE_k \quad \text{with} \quad \gamma_{ijkl} = \frac{\partial^2\varepsilon_{ij}^{\mathrm{T}}}{\partial E_k \partial E_l} \tag{7}$$

Cubic and higher order contributions of the electric field to the total strain are neglected, but can be incorporated into the formulation.

An alternative description of the quadratic contribution to strain from an electric field is described in terms of the polarization vector $\vec{P}$, where the corresponding electrostrictive tensor, Q_{ijkl}, relates strain to polarization change:[24,25,§]

$$\varepsilon_{ij}^{\text{electrostrictive}} = Q_{ijkl}P_kP_l \quad \text{with} \quad Q_{ijkl} = \frac{\partial^2\varepsilon_{ij}^{\mathrm{T}}}{\partial P_k \partial P_k} \tag{8}$$

By expanding

$$\gamma_{ijkl} = \frac{\partial d_{ijk}}{\partial E_l} = \frac{\partial}{\partial E_k}\left(\frac{\partial \varepsilon_{ij}^{\mathrm{T}}}{\partial P_n}\frac{\partial P_n}{\partial E_l}\right) \tag{9}$$

an electric field representation can be related to a polarization field:

$$\gamma_{ijkl} = Q_{ijmn}\kappa_{km}^{\sigma}\kappa_{nl}^{\sigma} + \Lambda_{knl}d_{mij}\beta_{mn}^{\sigma} \tag{10}$$

where

$$\kappa_{ij}^{\sigma} \equiv \epsilon_{ij}^{\sigma} - \epsilon_0\delta_{ij} \tag{11}$$

and

$$\beta_{in}^{\sigma}\epsilon_{jn}^{\sigma} \equiv \delta_{ij} \tag{12}$$

Here, $\delta_{ij} = 1$ if $i = j$ and zero otherwise.

For systems in which electro-optic effects can be neglected, the dielectric and piezoelectric tensors take the following form:[¶]

$$d_{ijk} = d_{ijk}^0 + Q_{ijmn}\kappa_{km}^{\sigma}\kappa_{nl}^{\sigma}E_l \tag{13}$$

and

$$\epsilon_{ij}^{\varepsilon} = \epsilon_{ij}^{\sigma,0} - d_{jmn}C_{mnkl}^{E}d_{ikl} + C_{ijkl}Q_{klpq}\kappa_{pr}^{\sigma}\kappa_{qs}^{\sigma}\varepsilon_{rs}^{\mathrm{T}} \tag{14}$$

(2) Plane-Stress Formulation

For a piezoelectric solid whose material properties are homogeneous out of a specified plane, such as in a ferroelectric film, the description of the local thermodynamic state of a polycrystalline solid can be reduced to a quasi-two-dimensional representation. For a piezoelectric material subjected to in-plane surface tractions and electric displacements, but free to deform out of the plane (i.e., in a state of plane stress), the electromechanical free energy density is[24]

$$f = \tfrac{1}{2}\varepsilon_{ij}^{\mathrm{T}}C_{ijkl}^{E}\varepsilon_{kl}^{\mathrm{T}} - \tfrac{1}{2}E_i\epsilon_{ij}^{\varepsilon^{\mathrm{T}}}E_j - E_ie_{ijk}\varepsilon_{jk}^{\mathrm{T}} \tag{15}$$

with

$$e_{ijk} \equiv C_{jklm}^{E}d_{ilm} \tag{16}$$

Define $\varepsilon_{ij}^{(2)}$ as the two-dimensional in-plane part of the strain with indices $i, j = \{1, 2\}$ (the out-of-plane index is taken as 3), and η_i as the out-of-plane components:

$$\overleftrightarrow{\varepsilon}^{\mathrm{T}} = \begin{pmatrix} \varepsilon^{(2)} & \eta_1 \\ & \eta_2 \\ \eta_1\ \eta_2 & 2\eta_3 \end{pmatrix} \tag{17}$$

For plane-stress conditions:

$$\sigma_{i3} = C_{i3kl}^{E}(\varepsilon_{kl}^{\mathrm{T}} - d_{mkl}E_m) = 0 \quad [i = 1, 2, 3] \tag{18}$$

Let $d_m^{(2)}$ be the two-dimensional in-plane contribution to the piezoelectric tensor

$$d_m = \begin{pmatrix} d_m^{(2)} & d_{m31} \\ & d_{m32} \\ d_{m31}\ d_{m32} & 2d_{m33} \end{pmatrix} \tag{19}$$

Here, d_{m3i} is the out-of-plane contribution to the piezoelectric tensor.

Equations (18) and (19) imply

$$C_{i3kl}^{E}\left(\varepsilon_{kl}^{(2)} - d_{mkl}^{(2)}E_m\right) = -2C_{i3j3}^{E}(\eta_j - d_{m3j}E_m) \quad [ikl = 1, 2 \text{ and } jm = 1, 2, 3] \tag{20}$$

which gives

$$\eta_i = -\frac{1}{2}\xi_{ij}C_{j3kl}^{E}\left(\varepsilon_{kl}^{(2)} - d_{mkl}^{(2)}E_m\right) + d_{m3i}E_m, \quad [ijm = 1, 2, 3 \text{ and } kl = 1, 2] \tag{21}$$

with $\xi_{ij}C_{j3kl}^{E} \equiv \delta_{ij}$. Using Eqs. (15), (16), and (21), f is

$$f = \frac{1}{2}\varepsilon_{ij}^{(2)}D_{ijkl}\varepsilon_{kl}^{(2)} - \frac{1}{2}E_i\chi_{ij}E_j - E_ie_{ijk}\epsilon_{jk}^{(2)} \tag{22}$$

where the plane-stress stiffness is

$$D_{ijkl} \equiv C_{ijkl}^{E} - C_{ij3n}^{E}\xi_{nm}C_{m3kl}^{E} \quad [ijkl = 1, 2 \text{ and } mn = 1, 2, 3] \tag{23}$$

and the plane-stress permittivity is

$$\chi_{ij} \equiv \epsilon_{ij}^{\varepsilon} + d_{i3m}C_{3m3n}^{E}d_{j3n} \quad [ij = 1, 2 \text{ and } mn = 1, 2, 3] \tag{24}$$

Equation (22) is the plane-stress analog to Eq. (15).

(3) Numerical Solution

The formulation described in Section 2.2 was implemented by applying the finite element method (see Appendix A). The numerical implementation results in a set linear equations (Eq. (22)) of the form $\mathbf{K}\vec{V} = \vec{b}$ in each degree of freedom. The final form of this matrix depends on the mesh and element properties. $\vec{V}$ is a vector with components corresponding to each unknown degree of freedom (nodal displacements and voltage) and $\vec{b}$ is a vector of the surface specified contributions from each degree of freedom (surface forces, electrostatic surface charges, boundary voltages and displacements). The global stiffness matrix, $\mathbf{K}$, is typically a sparse $M \times M$ matrix and can be determined *a priori*, in the linear case. M corresponds to the number of degrees of freedom not determined by the boundary conditions in the system.

[§]The polarization vector is related to the applied electric field $\vec{E}$ and total polarization $\vec{D}$ by:

$$P_i = D_i - \epsilon_0 E_i$$

where ϵ_0 is the permittivity of vacuum.

[¶]Because this is an expansion about a stable state, it is implicit that hysteretic effects, domain wall motion, charge separation, mass diffusion, and other irreversible kinetic effects cannot be operative, thus these equations apply. In a ferroelectric, there may be irreversible phase transitions that include switching events and local motion of domains.

The global solution can be obtained by a suitable numerical method for solving large sparse linear systems. The current implementation utilizes the conjugate gradient method.[26] The solution is an approximation in two senses. The first is the numerical approximation to the linear system of equations and the second is due to discretization. The quality of the solution to the linear equations is ensured by requiring that the residual $r = |\mathbf{K}\vec{V} - \vec{b}|/|\vec{b}|$ is less than a specified tolerance.[27] A maximum value of r is specified prior to solution. With regard to discretization, a numerical solution should capture the relevant features and variations of the fields and asymptotically converge to the exact solution with mesh refinement.

In the case of a material microstructure with local field-dependent properties, the form of the global equilibrium equation has a similar form, but is generally non-linear (i.e., the stiffness matrix depends on the (unknown) solution), $\mathbf{K}(\vec{V})\vec{V} = \vec{b}(\vec{V})$. In this case, a solution is obtained by applying Newton's method.[28] Newton's method has quadratic convergence. Other techniques for solving non-linear systems, such as the Picard and the Modified Newton's, were tried but did not converge as fast as Newton's method.[27,28,‖]

III. Model Validation and Discussion

(1) Model Implementation

The framework described in the sections above was implemented by modifying the Object Oriented Finite Element program (OOF), version 1.[29] OOF is a freely available software developed at NIST for the analysis of properties of microstructures. Because OOF is designed to operate on two-dimensional geometries, such as those from microstructural images these modifications permit solutions for arbitrary two-dimensional microstructures of piezoelectric phases with spatially variable crystallographic orientation. The solutions consist of both electric and mechanical fields. The additions to the code enlarge the variety of physical behaviors that can be calculated by the OOF program.[††] Examples of such calculations in a polycrystalline microstructure are given in a companion paper.[18] In this section, we demonstrate that the method is numerically stable and converges to known solutions for simple cases.

The modified version of OOF is applicable to systems where the electric field does not vary out of the plane. This is a valid assumption for materials whose dielectric tensor coefficients are much larger than the surrounding medium, e.g., an order of magnitude larger. Therefore, the modified code is applicable for thin film microstructures embedded in a low dielectric constant medium, such as vacuum.

(2) Homogeneous Materials

The numerical model was applied to a square, 1 m × 1 m single-crystal thin-film piezoelectric with isotropic dielectric properties to demonstrate that it yields sensible results. Piezoelectric coefficients correspond to Barium Titanate (point group 4*mm*).[30,31] Crystals belonging to the 4*mm* point group have three independent piezoelectric coefficients: d_{33}, d_{31}, and d_{15} in Nye's matrix notation.[23] Small values for the elastic tensor coefficients were selected to distinguish contributions between the direct and converse piezoelectric effects. The material properties are summarized in Table II. A 100 V potential difference was applied between the two edges with normals oriented in the positive and negative x-directions. All four in-plane edges were free to elastically deform in two dimensions. The material was also free to deform out of the plane. The crystal was oriented such that its c-axis remained in-plane at a counterclockwise angle θ with respect to the x-axis of the laboratory reference system. The equilibrium elastic and electric fields were calculated within OOF as a function of crystal orientation θ.

Table II. Physical Properties for Hypothetical Single-Crystal, Piezoelectric Solid. Piezoelectric coefficients correspond to $BaTiO_3$.

Symbol	Value	Units	Symbol	Value	Units
C_{11}	2.751	Pa	d_{31}	−34.7	pC/N
C_{33}	1.649	Pa	d_{33}	85.7	pC/N
C_{44}	0.543	Pa	d_{15}	392.0	pC/N
C_{12}	1.789	Pa	ϵ_{11}^{σ}	10.0	μF/m
C_{13}	1.516	Pa	ϵ_{33}^{σ}	10.0	μF/m

The exact and numerical solutions for this case have uniform electric and strain field distributions. Figure 1 compares the numerical and analytic solutions for angular variations of the uniform piezoelectric strains ε_{ij}, normalized by their values at θ = 0. The normalized angular dependencies have exact expressions:

$$\frac{\varepsilon_{11}}{d_{33}E_1} = \cos^3\theta + \frac{d_{15}+d_{31}}{d_{33}}\sin^2\theta\cos\theta \tag{25}$$

$$\frac{\varepsilon_{22}}{d_{31}E_1} = \cos^3\theta + \frac{d_{33}-d_{15}}{d_{31}}\sin^2\theta\cos\theta \tag{26}$$

$$\frac{\varepsilon_{33}}{d_{31}E_1} = \cos\theta \tag{27}$$

The absolute value difference between the analytical and OOF predictions is shown in Fig. 2.

The simulation results were computed on 5 × 5 node regular meshes.[‡‡] The tolerance was set to $r = 1 \times 10^{-12}$. Each simulation required about a million floating point operations (1 Mflop) for convergence (1 ms on an SGI Origin 2000).

To demonstrate the convergence of the non-linear case, an electrostrictive system ($BaTiO_3$, point group *m*3*m*, properties in Table III) was simulated. The solution was obtained for a square domain (1 mm × 1 mm). The c-axis was oriented parallel to the x-direction. A voltage difference along the x-direction was

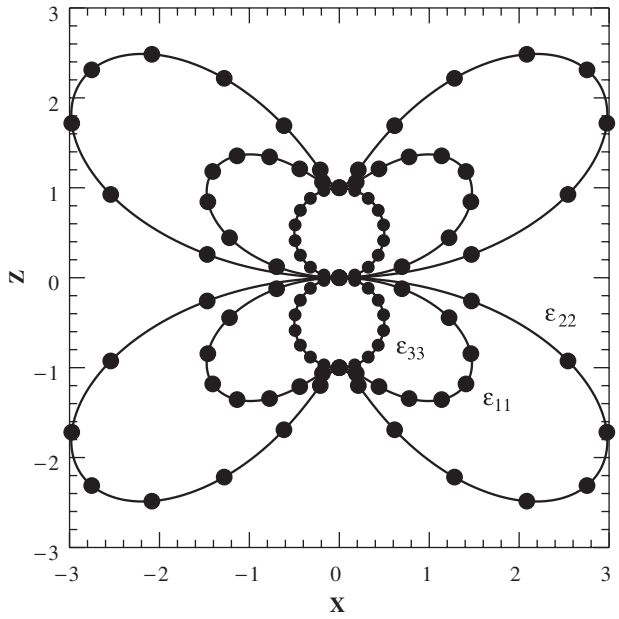

Fig. 1. Angular dependence of three contributions to normalized strain, ε_{11}, ε_{22}, and ε_{33}, (out-of-plane). Solid lines correspond to analytic predictions; dots show the Object Oriented Finite Element program solution.

‖The solution was obtained by solving the global equilibrium equation with an initial trial solution vector $\vec{V}_0$ for $\vec{V}_1$ to a tolerance r_L: $|\mathbf{K}(\vec{V}_0)\vec{V}_1 - \vec{b}(\vec{V}_0)|/|\vec{b}(\vec{V}_0)| \le r_L$. The global equilibrium equation was iterated ($|\mathbf{K}(\vec{V}_{N-1})\vec{V}_N - \vec{b}(\vec{V}_{N-1})|/|\vec{b}(\vec{V}_N)| \le r_L$) to find $\vec{V}_N$ until a non-linear tolerance $|\mathbf{K}_N\vec{V}_N - \vec{b}_N|/|\vec{b}_N| \le r_{NL}$.

††A new version of OOF, currently under development, will address piezoelectric microstructures without significant modifications.

‡‡Because the system lacks an implicit length scale, the obtained results are independent of mesh resolution. Below, a simulation is presented that incorporates a length scale that permits evaluation of mesh refinement.

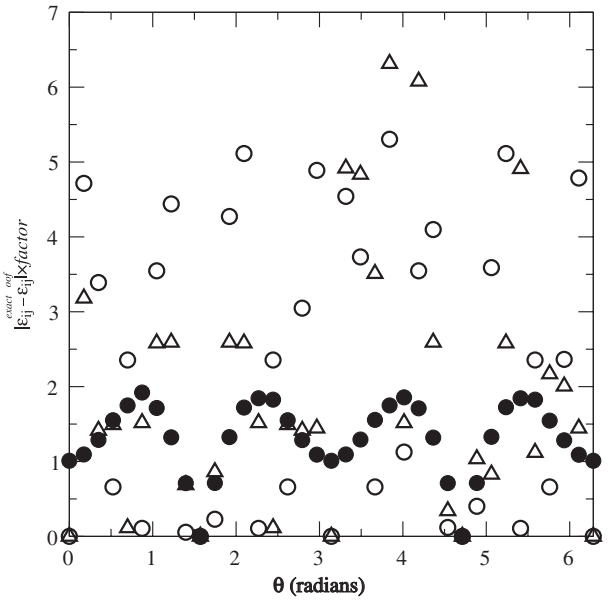

Fig. 2. Absolute value difference between Object Oriented Finite Element program and analytical predictions to piezoelectric strain (see Eqs. (25)–(27)). Filled circles correspond to ε_{11} with a multiplying factor of 1×10^4, ε_{22} to open circles with a multiplying factor of 1×10^5, and triangles to ε_{33}, with a scaling factor to 1×10^7.

applied in steps of 10 V ranging from −100 to 100 V; the sides parallel to the *x*-axis are electrically unconstrained. All edges are mechanically unconstrained.

By applying Eq. (13), and assuming that $d^0_{ijk} = 0$ (the case for point group *m3m*) the strain in the direction of an electric field applied along the *x*-direction is

$$\varepsilon_{11} = (\epsilon^{\sigma}_{11} - \epsilon_0)^2 Q_{11} E_1^2 \tag{28}$$

The electrostrictive constant is given in matrix notation.[23]

Linear and non-linear tolerances were set to $r_L = 10^{-4}$ and $r_{NL} = 10^{-7}$, respectively. The domain was divided in a uniform mesh with a total of 25 nodes. Each simulation took on the order of four Newton steps to converge. Each Newton step took on the order of 1 Mflop. A comparison between the OOF calculation and the exact response is shown in Fig. 3.

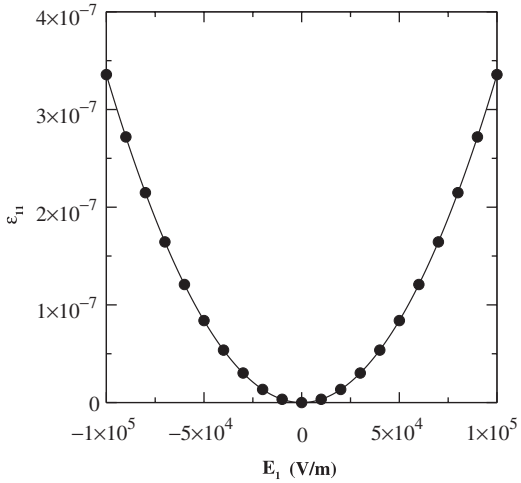

Fig. 3. Comparison between analytical and numerical electrostrictive response. Solid line corresponds to analytic response (Eq. (28)). Circles correspond to the Finite Element calculation.

IV. Convergence with Discretization

To assess discretization effects (i.e., mesh refinement), a simulation length scale is required for comparison with mesh size. Two hypothetical linear piezoelectric devices with such length scales were simulated (see Figs. 4 and 6). The simulated actuators will be referred to as anti-parallel and dead-layer devices, respectively.

The anti-parallel device (Fig. 4) is composed of two otherwise identical piezoelectric layers with anti-parallel *c*-axes. They are 1.0 mm long and 0.25 mm thick. Their material properties correspond to point group *4mm* and are summarized in Table II. The layers are perfectly bonded. The left edge of both layers is perfectly clamped to an infinitely stiff perfect conductor. The right side of the bilayer is bonded to a perfectly compliant (zero stiffness) perfect conductor.

Table III. Physical Properties Used in Single-Crystal Calculations for Electrostrictive $BaTiO_3$[30,32,33]

Symbol	Value	Units
C_{11}	172.80	GPa
C_{12}	81.96	GPa
C_{44}	108.22	GPa
Q_{11}	11.1×10^{-2}	m^4/C^2
Q_{12}	-4.42×10^{-2}	m^4/C^2
Q_{44}	5.85×10^{-2}	m^4/C^2
ϵ^{σ}_{11}	17.4	μF/m

Numerical solutions for the deflection of the bilayer appear in Fig. 5 as a function of mesh refinement. The highest resolution mesh (16 384 nodes, 49 152 degrees of freedom) required 5152 iterations to converge (a total of 4×10^5 Mflops). The meshes with the coarsest resolution (20 nodes, 48 degrees of freedom) required 23 iterations to converge (a total of 7.5 Mflops). The convergence tolerance was 1×10^{-12} for all refinements. Figure 5 suggests that approximately 32 elements across the characteristic length scale is sufficient for convergence.[§§]

In the anti-parallel piezoelectric device, a non-zero electric field component perpendicular to the applied voltage difference is observed. In this device, when a voltage difference is applied, the converse piezoelectric effect induces a change of shape in the *y* and *z* directions, which correspond to crystallographically allowed contributions to the contraction/expansion at these

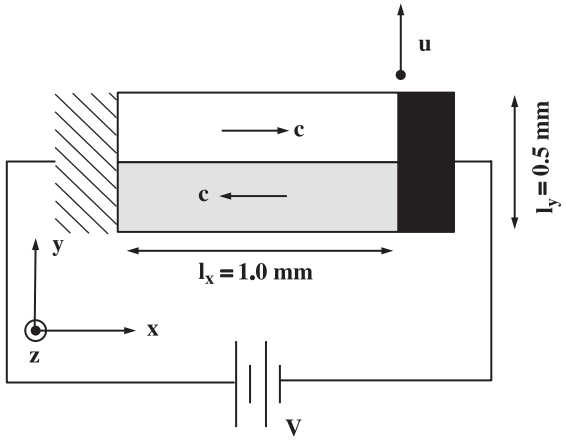

Fig. 4. Schematic representation of anti-parallel device. The left side is clamped to an infinitely stiff contact. The right side is mechanically free. The bilayer is composed of two oppositely poled layers of total in-plane thickness l_y, and equal length l_x. Upon applying a voltage difference, the bilayer bends displacing the upper right corner a distance *u*.

[§§]The number and distribution of elements required to reach a valid calculation depends on the studied geometry or microstructure, boundary conditions, materials properties, etc. Application of more sophisticated techniques such as mesh refinement algorithms to resolve for large localized spatial gradients improves the solution greatly.

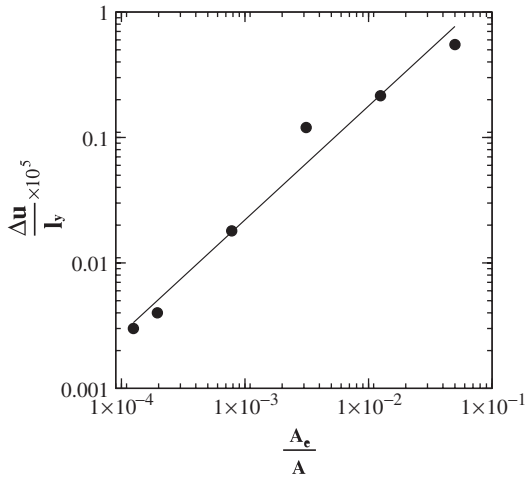

Fig. 5. Bending of piezoelectric anti-parallel device as a function of normalized element size. The normalization factor, A, is the total area of the bilayer. The y-axis is the difference between the vertical deflection of the bilayer device, for a particular mesh size, and the asymptotic solution, normalized by the thickness of the bilayer. The solid line is the regression curve of the convergence rate: $\frac{\Delta u}{l_y} \times 10^5 = 11.628(A_e/A)^{0.97}$.

boundaries. Via the direct piezoelectric effect, the material's deformation induces a change of polarization at the interface, which in turn induces a non-zero contribution to the electric field, perpendicular to the externally applied voltage difference.

The anti-parallel device is an inefficient piezoelectric actuator—its geometrical arrangement induces a large amount of stored mechanical energy at the interface. These localized mechanical and electrical energy densities could cause depoling, particularly for those transducers operating at temperatures close to the Curie temperature. Away from the Curie temperature, localized mechanical energy density distributions affect mechanical reliability.

The second piezoelectric transducer, the dead-layer device, is a piezoelectric strip perfectly bonded to a non-piezoelectric, metallic substrate (Fig. 6). The bottom layer is a perfectly conducting isotropic material with Young's modulus of 100 GPa and Poisson's ratio of 0.33. The c-axis of the piezoelectric layer makes an angle of 54.74° with respect to the laboratory y-axis. This orientation was chosen to maximize the single-crystal piezoelectric response observed in Fig. 1.

The numerical error in bending of the dead-layer device can be observed in Fig. 7 as a function of element size. The solution

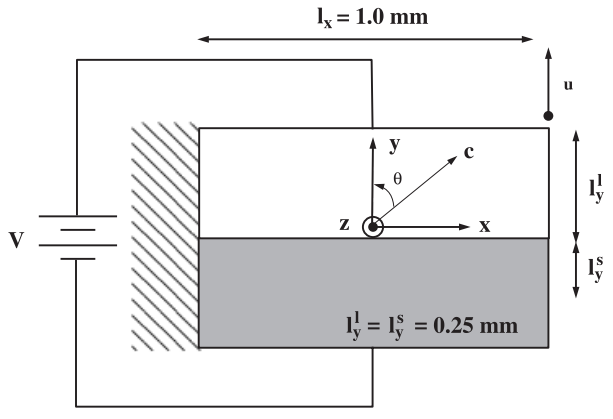

Fig. 6. Schematic of bilayer (dead-layer) system. Left side is clamped to an infinitely stiff contact. The right edge deforms freely. The device is composed of two layers of thickness l_y^s for the substrate and l_y^l for the piezoelectric layer. The length of the device is l_x. The substrate is a perfect metallic conductor. Upon applying a voltage difference, the bilayer bends displacing the upper right corner a distance u. The angle of the c–axis with respect to the y–axis of the laboratory reference system was set to provide a larger displacement than the anti-parallel device.

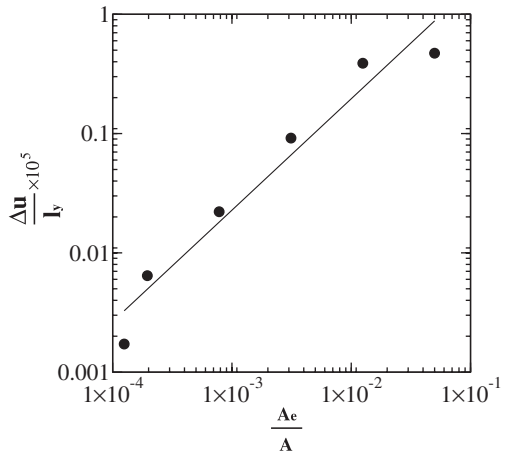

Fig. 7. Normalized vertical displacement of the upper-right corner in dead-layer piezoelectric device as a function of normalized element size. Here $\frac{\Delta u}{l_y} \times 10^5 = 14.432(A_e/A)^{0.934}$.

for the coarsest mesh (20 nodes, 48 degrees of freedom) required about 2.5 Mflops. The solution for the finest mesh (16 384 nodes, 49 152 degrees of freedom) required about 1200 Mflops.

Compared with the anti-parallel piezoelectric device, no residual, lateral electric fields (in directions perpendicular to the applied voltage difference) are produced. The electrical energy necessary to displace this actuator is less than the contributions from the anti-parallel device.

The magnitudes of the electric and stress fields in the dead-layer device reaches their maximum value at the interface of the active layer, particularly where the internal boundary meets the surface of the device. Here, the local properties mismatch and boundary conditions induce the observed effect. Therefore, polarization domain switching and mechanical failure is favored to initiate at the surface and interface of the device. The maximum displacement in the dead-layer device is maximized by the choice of orientation of the c-axis.

V. Summary and Conclusions

A model and numerical framework was established for the solutions of equilibrium electric and mechanical fields. The numerical implementation provides a method for calculating the response of a two-dimensional device as a function of its boundary conditions and geometry. Linear and quadratic representations of piezoelectric material properties were developed and provide a second-order model for reversible electromechanical materials. The solutions are accurate and consistent with simple geometries for which analytic solutions were derived. Numerical solutions were obtained for specific piezoelectric layer-like geometries. The geometries provide a length scale that can be used as a normalizing parameter to test numerical convergence with respect to mesh refinement. This convergence criteria is used in a continuing paper as a reference length scale to establish the validity of the calculations.[18]

The electromechanical response was compared for two hypothetical piezoelectric devices. The analysis suggests the response of these types of devices can be optimized by orienting the c-axis to a value that maximizes their response.

Surfaces and internal interfaces play an important role in determining the response of a piezoelectric device. A specific microstructure and well-determined applied fields lead to a distribution of mechanical and electrical energy that impacts directly on the life and reliability of the device; advanced actuator devices can benefit from such analyses.

The results for simple geometries in this paper are useful for developing design strategies for piezoelectric devices and can be summarized as follows:

(1) The macroscopic response of a piezoelectric actuator is a result of the spatial contributions from the direct and converse

piezoelectric effect. For a specific electromechanical transducer, the resulting electric and strain fields are a consequence of the spatial interactions of the inherent geometrical features (microstructure) and result in fields in directions that may not be parallel to the macroscopic applied field.

(2) Coherent internal interfaces where piezoelectric properties change discontinuously will result in regions of large elastic energy density and potentially affect mechanical reliability.

(3) The spatial incompatibility of elastic, dielectric, and piezoelectric properties results in localized spatial regions of electrostatic and elastic energy, which are favorable sites for depoling of the device.

(4) A sensible choice for the numerical value and crystallographic orientation of the utilized piezoelectric materials for single-crystal devices will maximize the macroscopic response and will minimize the induced mechanical energy distribution.

One of the main benefits of this modified version of OOF is its ability to easily capture complex microstructural features through simple point-and-click operations. Thus, this framework permits the description of a wide variety of microstructural features, such as pore and crack distributions, electromechanically dead layers, and interactions with static ferroelectric domains.

A further extension of this framework to account for spatial charge distributions and its impact on the local fields is easily included. Such addition only requires the full form of Coulomb's Law, i.e., $\nabla \cdot \vec{D} = \rho$, as well as the relevant constitutive thermodynamic relations already established in Section 2.[34] Similarly, the description of static (and pinned) domains can be readily assessed, by automatically identifying these microstructural features on a scanned micrograph (i.e., by carefully identifying the local Euler angles of each variant). Furthermore, the thermodynamic equilibrium of the underlying ferroelectric domains can be explored. Here, the local state of a volume element of material is determined by the electromechanical Gibbs free energy. If this free energy reaches a local maximum value (specified by the material's single-crystal coercive electric field or stress tensor) the element will attempt to acquire an orientation that simultaneously decreases the local free energy. A Monte Carlo algorithm, similar to the one utilized for other instances of OOF (e.g., *Kessler, Griffith*, or *Valeria* elements) will easily incorporate these ideas.[29] However, the imposed constitutive laws should comply with the crystallographic constraints imposed by the parent phase and the involved variants of the ferroelectric phase.[19,35]

The results in this paper establish the validity of the numerical method and its convergence behavior. The convergence to known solutions provides confidence that application of this numerical model to complex microstructures will provide a valid solution where analytical solutions are impossible. Thus, this paper establishes the groundwork for the numerical method for analysis of microstructural properties that is utilized in the companion paper.[18]

Appendix A. Finite Element Formulation

In the absence of body forces and localized electrostatic charges, the virtual change in the electromechanical free energy is:[36]

$$\int_{\Omega} (\vec{\vec{\sigma}}\delta\vec{\vec{\varepsilon}} - \vec{D}\cdot\delta\vec{E})\mathrm{d}\Omega = \int_{S^M} \delta\vec{X}\cdot\vec{\vec{\sigma}}\cdot\vec{n}\mathrm{d}S + \int_{S^E} \delta\phi\vec{D}\cdot\vec{n}\mathrm{d}S \tag{35}$$

where Ω is the volume with bounding surface S with unit normal $\vec{n}$. The subsets of S (S^M and S^E) where mechanical tractions ($\vec{\sigma}\cdot\vec{n}$) and surface charge ($\vec{D}\cdot\vec{n}$) are specified may overlap. The strain, $\vec{\vec{\varepsilon}}$, and electric field, $\vec{E}$, are functions of the spatial derivatives of the displacement field $\vec{u}$ and electrostatic potential ϕ.

Table IV. Physical Properties for Barium Titanate Used in Calculations of Piezoelectric Bending Devices (Anti-Parallel and Dead-Layer)[30,31]

Symbol	Value	Units	Symbol	Value	Units
C_{11}	275.1	GPa	d_{31}	−34.7	pC/N
C_{33}	164.9	GPa	d_{33}	85.7	pC/N
C_{44}	54.35	GPa	d_{15}	392.0	pC/N
C_{12}	178.9	GPa	ϵ^{σ}_{11}	17.442	μF/m
C_{13}	151.6	GPa	ϵ^{σ}_{33}	0.965	μF/m

Table V. Glossary of Used Symbols in Finite Element Numerics

Summary of symbols for implemented finite element method	
Definition	Name
$\mathbf{B}^m_j$	Displacement-to-strain conversion matrix
D_{ijkl}	Two-dimensional stiffness tensor. For a solid under plane-stress conditions, D_{ijkl} is given by Eq. (23)
$\mathbf{G}^m_j$	Finite element gradient vector mth Element, jth node (see Zienkiewicz)[26]
$\mathbf{K}$	Total stiffness matrix
$\mathbf{K}_m$	Stiffness matrix (defined by Eq. (36))
N^m_i	Trial function in mth element, ith node
P	Number of nodes in element
a^m_j, b^m_j, c^m_j	Trail function coefficients in triangular mth element, jth node
$\vec{b}$	Total body force
$\vec{u}$	Total degrees of freedom vector
$\vec{u}_m$	Vector of degrees of freedom (contains the mth element voltage and displacement fields)
x^m_j, y^m_j	Nodal positions of jth node, mth element
Δ	Area of triangular element
$\delta\phi$	Electric potential test function
ϕ^m	Finite element approximation to electric potential in mth element
ϕ^m_i	Nodal electric potential in mth element, ith node
χ_{ij}	Effective two-dimensional permittivity matrix. The explicit form is given by Eq. (24)

The finite element approximation is introduced by discretizing the domain (volume) into a complete set of non-overlapping homogeneous subregions (elements). Each element is connected to its neighbors through shared discrete values (nodes). Within each element, n, the fields are described by linear combinations of functions N^n_j (shape functions).[¶¶] Substitution of N^n_j into Eq. (21) reduces the integral to a set of coupled linear equations.[28,37]

By substituting the two-dimensional electromechanical properties derived in Section II into Eq. (21) one finds for the case of linear triangular elements:[|||]

$$\Delta\begin{pmatrix} B^{\nu}_{ij}D_{ijkl}B^{\mu}_{kl} & -B^{\nu}_{ij}e_{mij}G^{\mu}_{m} \\ -G^{\nu}_{i}e_{ijk}B^{\mu}_{jk} & -G^{\mu}_{i}\chi_{ij}G^{\nu}_{j} \end{pmatrix}\begin{pmatrix} \vec{u}^{\mu} \\ \phi^{\mu} \end{pmatrix} = \begin{pmatrix} (\vec{\vec{\sigma}}\cdot\vec{n})_{S^M} \\ (\vec{D}\cdot\vec{n})_{S^E} \end{pmatrix} \tag{36}$$

where μ and ν are the indices for each node in the element (i.e., μ, ν = 1, 2, 3 for triangular elements). The symbols are defined in Table V.

[¶¶] The shape function N^n_j interpolates within the values associated with each of its nodes; it is unity at node j and zero at the other nodes.

[|||] The algebraic details of the derivation of the final equations is omitted here but is a direct extension of the treatment in standard finite element method texts.[36–38]

Acknowledgments

Many thanks to Dr. Catherine M. Bishop for the helpful discussions and for reading this manuscript.

References

[1]K. Uchino, "Piezoelectric Actuators/Ultrasonic Motors—Developments and Markets;" pp. 319–324 in *Proceedings of the Ninth IEEE International Symposium on Ferroelectrics, ISAF 94*. IEEE, University Park, PA, 1994.

[2]J. W. S. Rayleigh, "On the Influence of Obstacles Arranged in Rectangular Order Upon the Properties of the Medium," *Philos. Mag*., **34**, 481–502 (1892).

[3]J. D. Eshelby, "The Determination of the Field of an Ellipsoidal Inclusion and Related Problems," *Proc. Roy. Soc. London A*, **241**, 376–96 (1957).

[4]R. Hill, "A Self Consistent Mechanics of Composite Materials," *J. Mech. Phys. Solids*, **13**, 213–22 (1965).

[5]B. Budiansky, "On the Elastic Moduli of Some Heterogeneous Materials," *J. Mech. Phys. Solids*, **13**, 223–7 (1965).

[6]Z. Hashin, "Analysis of Composite Materials," *J. Appl. Mech*., **50**, 481–505 (1983).

[7]W. F. J. Deeg, "The Analysis of Dislocation, Crack, and Inclusion Problems in Piezoelectric Solids." Department of Materials Science and Engineering, Stanford University, PhD Thesis. 1980.

[8]M. Marutake, "A Calculation of Physical Constants of Ceramic Barium Titanate," *J. Phys. Soc. Japan*, **11** [8] 807–14 (1956).

[9]N. A. Pertsev, "Aggregate Linear Properties of Ferroelectric Ceramics and Polycrystalline Thin Films: Calculation by the Method of Effective Piezoelectric Medium," *J. Appl. Phys*., **84** [3] 1524–9 (1995).

[10]N. A. Pertsev, A. G. Zembil'gotov, and R. Wazer, "Effective Dielectric and Piezoelectric Constants of Thin Polycrystalline Ferroelectric Films," *Phys. Solid State*, **40** [12] 2002–8 (1998).

[11]S. Hwang, J. E. Huber, R. E. McMeeking, and N. A. Fleck, "The Simulation of Switching in Polycrystalline Ferroelectric Ceramics," *J. Appl. Phys*., **84** [3] 1530–40 (1998).

[12]W. Kreher and J. Rodel, "Ferroelectric Ceramics and Composites: Statistical Models for Effective Piezoelectric and Pyroelectric Properties;" pp. 455–458 in *Applications of Ferroelectrics, 1998. ISAF 98. Proceedings of the Eleventh IEEE International Symposium on Ferroelectrics*, Edited by E. Colla, D. Damjanovic, and N. Setter. Institute fur Werkstoffwissenschaft, Technical University Dresden, Germany, 1956.

[13]T. Olson and M. Avellaneda, "Effective Dielectric and Elastic Constants of Piezoelectric Polycrystals," *J. Appl. Phys*., **71** [9] 4455–64 (1992).

[14]M. L. Dunn, "Effects of Grain Shape Anisotropy, Porosity, and Microcracks on the Elastic and Dielectric Constants of Polycrystalline Piezoelectric Ceramics," *J. Appl. Phys*., **78** [3] 1533–41 (1995).

[15]V. Aleshin, "Properties of Anisotropic Piezoactive Polycrystals," *J. Appl. Phys*., **88** [6] 3587–91 (2000).

[16]J. Y. Li, "The Effective Electroelastic Moduli of Textured Piezoelectric Polycrystalline Aggregates," *J. Mech. Phys. Solids*, **48**, 529–52 (2000).

[17]C.-W. Nan and D. R. Clarke, "Effective Properties of Ferroelectric and/or Ferromagnetic Composites: A Unified Approach and its Application," *J. Am. Ceram. Soc*., **80**, 1333–40 (1997).

[18]R. E. García, W. C. Carter, and S. A. Langer, "The Effect of Texture on the Macroscopic Properties of Polycrystalline Piezoelectrics: Applications to Barium Titanate and PZN-PT," *J. Am. Ceram. Soc*., **88**, 750–7 (2005).

[19]E. K. H. Salje, *Phase Transitions in Ferroelastics and Co-Elastic Crystals*. Cambridge University Press, Cambridge, UK, 1990.

[20]R. D. James and K. F. Hane, "Martensitic Transformations and Shape Memory Materials," *Acta Mater*., **48** [1] 197–222 (2000).

[21]H. F. Tiersten, *Linear Piezoelectric Plate Vibrations. Elements of the Linear Theory of Piezoelectricity and the Vibrations of Piezoelectric Plates*. Plenum Press, New York, 1969.

[22]R. E. García, C. M. Bishop, and W. C. Carter, "Thermodynamically Consistent Variational Principles with Applications to Electrically and Magnetically Active Systems," *Acta Mater*., **52**, 11–21 (2004).

[23]J. F. Nye, *Physical Properties of Crystals. Their Representation by Tensors and Matrices*. Oxford University Press, Oxford, UK, 1998.

[24]T. Ikeda, *Fundamentals of Piezoelectricity*. Oxford University Press, Oxford, UK, 1996.

[25]G. H. Haertling, "Ferroelectric Ceramics. History and Technology," *J. Am. Ceram. Soc*., **82**, 797–818 (1991).

[26]R. Barrett, M. Berry, T. F. Chan, J. Demmel, J. Donato, J. Dongarra, V. Eijkhout, R. Pozo, C. Romine, and H. Van der Vorst, *Templates for the Solution of Linear Systems: Building Blocks for Iterative Methods*, 2nd edition, SIAM, Philadelphia, PA, 1994.

[27]G. Strang, *Introduction to Applied Mathematics*. Wellesley-Cambridge Press, Wellesley, MA, 1986.

[28]O. C. Zienkiewicz and R. L. Taylor, *The Finite Element Method*, **Vol. 2**. Butterworth-Heinemann, Oxford, 2000.

[29]S. A. Langer, W. C. Carter, and E. R. Fuller, "OOF: Analysis of Real Material Microstructures," 2004. http://www.ctcms.nist.gov/oof/

[30]F. Jona and G. Shirane, *Ferroelectric Crystals*. Dover Publications Inc, New York, USA, 1993.

[31]A. E. Giannakopoulos and S. Suresh, "Indentation of Piezoelectric Materials;" in *Theory of Indentation of Piezoelectric Materials*. Laboratory for Experimental and Computational Micromechanics, 1999.

[32] Berlincourt and Jaffe, "Elastic and Piezoelectric Coefficients of Single-Crystal Barium Titanate," *Phys. Rev*., **111** [1] 143–8 (1958).

[33]M. J. Haun, E. Furman, S. J. Jang, and L. E. Cross, "Modeling the Electrostrictive, Dielectric, and Piezoelectric Properties of $PbTiO_3$," *Trans. Ultrasonics Ferroelectrics Frequency Control*, **36** [4] 393–401 (1989).

[34]J. D. Jackson, *Classical Electrodynamics*. Wiley, New York, 1975.

[35]Y. C. Shiu and K. Bhattacharya, "Domain Patterns and Macroscopic Behavior of Ferroelectric Materials," *Philos. Mag. B*, **81** [12] 2021–54 (2001).

[36]H. Allik and T. J. R. Hughes, "Finite Element Method for Piezoelectric Vibration," *Int. J. Numer. Meth. Eng*., **2** [1] 151–7.

[37]O. C. Zienkiewicz and R. L. Taylor, *The Finite Element Method*, **1**. Butterworth-Heinemann, Oxford, 2000.

[38]P. Gaudenzi and K.-J. Bathe, "Recent Applications of an Iterative Finite Element Procedure for the Analysis of Electroelastic Materials;" pp. 59–70 in *Fourth International Conference on Adaptive Structures*, Edited by E. J. Breitbach, B. K. Wada, and M. C. Natori. Technomic Publishing Co. Inc., Adam Hilger, Boston, 1993. □